Journal of Thermal Analysis and Calorimetry, Vol. 59 (2000) 227–243

Dedicated to Prof. Edith A. Turi in recognition of her leadership in education

TMDSC AND ATOMIC FORCE MICROSCOPY STUDIES OF MORPHOLOGY AND RECRYSTALLIZATION IN POLYESTERS INCLUDING ORIENTED FILMS

B. B. Sauer, W. G. Kampert, R. S. McLean and P. F. Carcia

DuPont Central Research & Development, Experimental Station, Wilmington, DE 19880-0356 USA

Abstract

The thermal and crystal morphological properties of poly[ethylene teraphthalate] (PET) and poly(ethylene-2,6-naphthalenedicarboxylate) (PEN) biaxially oriented films were compared to amorphous and other isotropic semi-crystalline samples. Crystal melting as a function of temperature was characterized by temperature modulated DSC (TMDSC) and found to begin just above the glass transition for both oriented films. About 75°C above the glass transitions, substantial exothermic recrystallization begins and continues through the final melting region in oriented films. The maximum in the non-reversing TMDSC signal for the oriented films signifies the maximum recrystallization exothermic activity with peaks at 248°C and 258°C for PET and PEN, respectively. The final melting endotherm detected was 260°C and 270°C for PET and PEN, and is shown by the TMDSC data and by independent rapid heating rate melting point determinations to be due to the melting of species recrystallized during the heating scan. The results are compared with TMDSC data for initially amorphous and melt crystallized samples. The volume fraction of rigid species (F_{rigid}=total crystal fraction plus 'rigid amorphous or non-crystalline species') were measured by TMDSC glass transition data, and contrasted with the area fraction of rigid species at the oriented film surface characterized with very high resolution atomic force microscopy (AFM) phase data. The data suggest that the 11 nm wide hard domains in PET, and 21 nm wide domains in PEN film detected by AFM consist of both crystal and high stiffness interphase species.

Keywords: atomic force microscopy (AFM), morphology, polyester, recrystallization, TMDSC

Introduction

Orientation, morphology, and thermal properties including the glass transition temperature (T_g) control properties [1] such as strength, permeability, modulus, dimensional stability, and toughness. Many of the elevated temperature properties can be related to recrystallization and other thermal events related to metastability [2] of polymer crystals. Temperature Modulated DSC (TMDSC) [3–6] is a newer technique which provides information on melting and recrystallization not accessible to standard DSC. To compare with the rich history of thermal and morphological character-

1418–2874/2000/ $ 5.00

Akadémiai Kiadó, Budapest

Kluwer Academic Publishers, Dordrecht

ization of aromatic polyesters, [2, 4, 7–15] we have chosen to study poly(ethylene terephthalate) (PET) and poly(ethylene-2,6-naphthalenedicarboxylate) (PEN).

In this work we will refer to the model of Zhou and Clough [10] for the description of multiple endotherms in DSC derived from DSC heating rate studies of isothermally crystallized PET. Their interpretation considers both dual crystal populations, early melting and recrystallization. A typical DSC curve for isothermally crystallized PET can be explained by early melting of secondary crystals which contribute to the low endotherm region, melting of primary crystals to the 'middle' endotherm which is always present but not always distinguishable, and the final endothermic region contains significant contributions from the recrystallized species formed during heating [10]. Support for the model is given by recent DSC/ X-ray studies [14, 16], TMDSC studies [15], and theoretical analysis of DSC curves [17].

TMDSC [3–6] gives improved information over that from standard DSC in quantifying the strength of broad and weak glass transitions in oriented films [4, 6] or highly crystalline samples.

The reversing signal separates the glass transition from other non-reversing processes such as enthalpy relaxation and exothermic crystallization [3–6]. Although exothermic events are detected in the NR-signal only, endothermic crystal melting contributes to both the reversing and non-reversing signals and one must choose experimental systems and conditions to estimate the various contributions.

There are many difficulties in obtaining accurate total crystallinities by various techniques. The DSC (or TMDSC) total heats of fusion are precise and can be converted into crystallinities using standard methods, and this will be critically evaluated here. The combination of rigid fraction determined by the strength of the glass transition [4, 12, 18], i.e., those species including the crystal phase and interphase species which cannot contribute to the glass transition, and the measured total crystallinities gives some information of mobile amorphous and rigid non-crystalline (rigid amorphous) fractions. These are then used to understand crystalline morphology, interphase properties, and other properties. Atomic force microscopy (AFM) also characterizes crystal and amorphous morphology, and we will show that some properties of interphase species can also be indirectly obtained if crystallinity is independently measured.

AFM investigations of morphology of semi-crystalline polymers [19–21] illustrate the excellent resolution of these techniques. Studies of isotropic polyesters are rare, but oriented PET film morphologies have been studied at very high resolution [22]. The effect of plasma etching has been studied [23], and correlation of longer range roughness from processing and film fabrication has also been characterized [22]. We are interested in applying tapping-mode® AFM, which is an intermittent contact method, for very high resolution studies of crystalline domains on oriented film surfaces. This method is optimum for high resolution studies because of negligible damage and deformation of the surface, and the AFM

phase data are sensitive to local stiffness differences of domains near the surface and have lateral resolution on the order of a nanometer for polymers.

Experimental

Materials and preparation

PET was obtained from DuPont with a weight average molecular weight (*Mw*) of 50,000 [14]. PEN with *Mw* of about 45,000 determined by viscosity, was obtained from Teijan Chemical Co. Poly(oxy-1,4-phenyleneoxy-1,4-phenylenecarbonyl-1,4-phenylene) (PEEK 150G) with a weight average molecular weight of about 30,000 was obtained from ICI, Ltd. Biaxially oriented PET and PEN were obtained from DuPont as Mylar® 400D and Kaladex® 1030, respectively. The draw ratios were about 3 in both directions, and non-isothermal crystallization temperatures were about 180°C for PET and 200°C for PEN.

Films 0.3 mm thick between sheets of releasing Kapton® polyimide were held in the melt in order to prepare isotropic films as was described previously [15]. PEN films were held at 290°C for 2 min, and PEN films at 280°C for 2 min followed by a rapid quench to 195°C for isothermal annealing for 1 to 3 h (Table 1).

The evaluation of $\Delta H_{f,o}$ for polymers is quite difficult. For PEN reported values are 102.5 [12] and 190 J g^{-1} [11] and for PEEK 130 J g^{-1} [24] and 160 J g^{-1} [25]. Although the discrepancies are greater for PEN, both will cause errors in calculation of absolute crystallinity, and also to all other related quantities such as rigid amorphous fractions. Measured densities for semi-crystalline samples also contribute to some variability in the determination of $\Delta H_{f,o}$, and there may also be some contribution of the accuracy of measured ΔH from DSC. Measured crystal densities by WAXD crystallography also can cause significant variability because the calculated $\Delta H_{f,o}$ requires extrapolation to the 100% crystalline density [11, 24]. Table 1 gives measured values for all quantities. Crystalline density (ρ_c) values were taken from the literature for PEEK [24, 26], PEN α-form (crystallized below 210°C) [11], and PEN β-form (crystallized above 210°C) [11]. Our amorphous value determined by chloroform density gradient column for PEN (ρ_a=1.3274 g cm^{-3}) can be compared with ρ_a=1.3400 g ml^{-1} from Buchner *et al.* [11]. This large difference mostly explains their higher value of $\Delta H_{f,o}$ =190 J g^{-1} compared to our value of 170±10 J g^{-1} (Table 2). Cheng *et al.* have obtained a value of $\Delta H_{f,o}$= 102.5 J g^{-1} [12]. As discussed by Buchner *et al.* [11], the crystal density of the α-form of PEN is ρ_c=1.407 g cm^{-3}, while for the high temperature β-form it is apparently 1.439 g cm^{-3}. For comparison purposes, using ρ_c=1.407 g cm^{-3} for a high temperature crystallized PEN sample gives $\Delta H_{f,o}$=159±10 J g^{-1}, while using ρ_c=1.439 g cm^{-3} gives an abnormally high value of $\Delta H_{f,o}$=225 J g^{-1} (Table 2). Either the crystallization conditions caused a mixture of crystal forms, or the value of ρ_c=1.439 g cm^{-3} is not accurate and is too high. For PEEK, the value of ρ_a=1.263 g cm^{-3} [24] compares well with our measured value of 1.2612±0.0002 g cm^{-3} (Table 2), and the value of ρ_c shows some variability de-

Table 1 Summary of DSC results

	ΔC_p 2 °C min^{-1}, 3.5 °C min^{-1}	T_g/°C	ΔH/J g^{-1} exo, NR	ΔH/J g^{-1} endo, NR	ΔH/J g^{-1} endo, R	ΔH/J g^{-1} total	F_{rigid}	Wc	F_{RAF}
Amorph PET	0.405[A]	77	118	0	120	2	0	0	0
Oriented PET	0.124, 0.102	94	31	94	0	62	0.73	0.45	0.28
195°C, 1 h melt crystallized	0.103	85	45	1	101	57	0.746	0.413	0.33
231°C , 24 h melt crystallized	0.0405	78	0	59	13	72	0.9	0.52	0.38
Amorph PEN	0.334[A]	123	108	0	108	0	0	0	0
Oriented PEN	0.051, 0.044	127	46	106	0	60	0.85	0.35	0.50
190°C, 3 h	0.111, 0.107	129	70	0	118	48	0.67	0.28	0.39

[A]Data taken at 3.5 °C min^{-1} are not reliable for ΔC_p for amorphous polymers because of the narrow temperature range over which the glass transition occurs for amorphous polymers. Our lower heating rate(2 °C min^{-1}) values of ΔC_p were consistent with the data in reference 28.
[B]The values for the exotherms(exo) and endotherms(endo) were obtained by standard integration using the software supplied with the instrument, and the choice of baselines shown in the figures.

pending on crystallization conditions. We have chosen a value of ρ_c=1.38 g cm^{-3} [26], giving a calculated $\Delta H_{f,o}$=163±15 J g^{-1} from our limited data. The results are consistent with that obtained from measured volume changes (160 J g^{-1}) using dilatometry [25]. The PEEK data are included here to illustrate the comparable values to PEN and also with PET which has $\Delta H_{f,o}$=138 J g^{-1} [27, 28]. There is good agreement between two different methods for PET [27, 28], but little agreement for many other polymers.

Table 2 Summary of densities and heat of fusion

	PEN				
	ρ_a/g cm^{-3}	ρ_c[A]/g cm^{-3}	ρ/g cm^{-3}	ΔH_f/J g^{-1}	$\Delta H_{f,o}$/J g^{-1}
190°C, 3 h	1.3274	1.407	1.3495	49±1	175
210°C, 2 h	1.3274	1.407	1.3567	65±2	175
240°C, 2 h	1.3274	1.407[B]	1.3569	59±1	159
240°C, 2 h	1.3274	1.439[C]	1.3569	59±1	225[C]
	PEEK				
270°C, 1.5 h	1.2612	1.38	1.3039	55±3	153
300°C, 2 h	1.2612	1.38	1.3023	60±2	173

[A]All values of ρ_c are taken from the literature. Ten samples were used for each determination of ρ_a, 5 samples for each annealing condition, and at least 3 samples for ΔH determination.
[B]α-form value of ρ_c was used even though this density is normally considered only for annealing below 210°C.
[C]β-form crystal density was used, giving abnormally high value of ΔH_o.

DSC

A TA Instruments (Newcastle, DE) 2920 DSC was used with signal processing provided by the manufacturer [29]. A standard heating ramp of 3.5°C min^{-1} was chosen and a modulation period of 60 seconds and a modulation temperature amplitude of 0.56°C was chosen based on the recommended specifications. To confirm the results, all systems were also characterized at 2°C min^{-1}, a modulation period of 60 seconds and a modulation temperature amplitude of 0.32°C . The total signal was almost the same for both underlying heating rates, but the separated reversing and non-reversing heats of fusion and melting were larger for the higher heating rate. Also, for measuring the strength of the glass transition of amorphous samples, only at the lower heating rate were a sufficient number of modulation cycles obtained for accurate characterization. At least four full cycles over the range of the glass transition are recommended [29].

Baseline calibration was performed regularly with empty pans at 2°C min^{-1} and 3.5°C min^{-1}, and a four point temperature calibration was performed with different metal standards. Careful baseline calibration is critical for these films exhibiting broad and weak transitions. The cell constant was calculated by standard analysis of an Indium standard, the heat capacity calibration constant for the modulation calibration was done using a standard sapphire sample [29]. To reduce heat flow lags, sample masses of 3–8 mg consisting of flat single layer polymer films were used. The

modulation temperature amplitude is small relative to the underlying heating rate, and the modulated profile is heating only. At steady state, the residual heat flow detected in the zero heating rate section of the modulation cycle can be used as a measure of a non-reversing exothermic or endothermic process [30].

Interpretation of TMDSC

The following is a brief summary of our current interpretation based on several experiments and systems designed to undergo various degrees of crystal reorganization during temperature scanning [15].

1. The non-reversing endothermic signal is typically due to complete melting of separate lamellae or stacks of lamellae and recrystallization cannot occur because the nuclei are lost or the barrier to recrystallization is too high because of low undercooling [6]. In the TMDSC analysis the melting kinetics must also be considered. If melting kinetics become so slow that melting occurs even during the zero heating rate part of the temperature modulation cycle, then such kinetic processes will contribute to a NR endotherm [29]. Annealing polyesters at high temperatures (within ca. 20°C of final melting point) results in species which melt at a low degree of undercooling (example given later). These crystals also tend to be susceptible to superheating because of their slow melting kinetics, contributing to a very large non-reversing melting endotherm for the same reason.

2. The reversing endothermic signal can be due to partial melting of lamellae followed by rapid recrystallization which occurs due to templating of just melted chains on existing lamellae [5]. This recrystallization occurs even though there is no local 'cooling' in the temperature modulated profile because we have chosen a small modulation amplitude relative to the underlying heating rate. Okazaki and Wunderlich show that in PET there is significant reversible melting because of 'molecular nucleation' [5, 6]. Molecular nucleation occurs when chains or chain segments melt near or on high-melting crystals, and then with negligible cooling, they can nucleate and recrystallize on these existing unmelted crystals. In addition to this contribution, in typical TMDSC temperature scans the reversing signal possibly contains a contribution from those species which are melting and recrystallizing independent of molecular templating. For example, many systems such as those discussed here exhibit low temperature melting and recrystallization, and the recrystallization is detected in the NR exothermic signal. The species which crystallize at low temperatures are metastable and the continuing process of melting and recrystallization of such species will contribute to a reversing endothermic signal regardless of whether molecular nucleation or recrystallization into entirely new lamellar stacks occurs. These contributions will help in the evaluation of the typical thermal scan. Recent work should be consulted concerning details of 'equilibrium' reversible melting as a function of different quasi-isothermal aging times where the sample is aged at long times [5], but much of the initial morphology is erased.

3. Exothermic crystallization events are detected in the non-reversing signal and not the reversing signal, making this a very powerful technique for separation of exotherms from glass transitions, reversible melting, or other heat capacity related

events. Exothermic and endothermic non-reversible events can both occur simultaneously and can offset each other. Because of this TMDSC data are difficult to interpret for many polymers [6, 15], especially those which are prone to recrystallization during the measurement.

Rapid heating rate technique

To measure the melting properties of crystals 'originally' present in the sample at heating rates fast enough to avoid recrystallization, a section of a sample (about 2 mg) is quickly pressed against a temperature controlled surface using a procedure described previously [15]. This is equivalent to measuring melting points under zero entropy production [1] and is determined by inspection of viscoelastic properties (flow) and verified by immediately quenching and measuring crystallinity of the particle by DSC or density [7]. One expects that the following measurement, done properly, will measure the temperature of the end of the melting range of crystals originally present in the sample without reorganization effects. Typically, the inspection of viscoelastic properties consists of quickly determining whether complete flow (liquification) of the entire sample occurs during the first fraction of a second, or in less obvious cases we examined the level of liquid transfer from the bottom of the sample to the metal surface.

AFM

AFM was performed using tapping mode* (Nanoscope 3A, Digital Instruments, Santa Barbara, CA) in air, using methods described previously [20, 31–33]. Tapping-mode is a contact technique, but the intermittent contact allows one to control the forces to very low levels and significantly reduce the lateral drag forces and surface damage compared to scanning 'contact' AFM [31].

Very sharp micro-fabricated tips (Digital Instruments, Santa Barbara, CA) with 6–10 nm radii of curvature were used. The tip is oscillated normal to the surface and is driven at a frequency close to the cantilever resonance frequency (300 kHz). As the tip is engaged on the surface, the frequency is positioned on the low frequency side of the resonance to prevent artifacts discussed in detail previously [32, 33]. The height data are measured by a feedback loop where the vertical distance is adjusted to keep the tip oscillation amplitude constant, and simultaneously the phase lag is measured between the tip driving signal and the actual tip response as it viscoelastically interacts with the surface. These 'phase' data are sensitive to local stiffness differences of species or domains near the surface. We use 'moderate force' tapping where the free air oscillation amplitude is reduced by about 40% upon engagement of the tip with the surface, as is discussed in previous work [31]. Under these 'moderate tapping force' conditions, hard domains have a larger phase lag [20, 21, 31–33] which is plotted as light regions. Experimental evidence obtained on these samples which includes variation of tip/sample forces by changing the tapping forces, suggest that there is a thin amorphous layer (1 nm thick) covering the entire surface. Unlike some other sys-

tems [20], in the oriented polyester films studied here the surface roughness including the protruding ~10 nm wide lamellae contribute to true high steps and are not caused by tip induced deformation of the surface. For example, in other systems such as copolymers the tip deformation causes soft regions to appear as lower spots, but at very low forces the height contrast approaches zero [33].

Results

The surface morphologies of biaxially oriented films are shown in Figs 1 and 2 where AFM height and phase data are obtained simultaneously during scanning, giving a one-to-one correspondence of the height and phase data in the figures. For these very high resolution images, in the phase data one observes hard domains slightly oriented in the original machine direction of the film (MD is horizontal direction in the figures). The slight orientation of the anisotropic lamellae in the horizontal direction is due to the sequential stretching process which consists of orientation in the transverse direction followed by final stretching in the machine direction. Boundaries between domains are dark and consist of softer (amorphous) material. The height data generally show that the high spots correspond to the hard domains, and contain similar in-

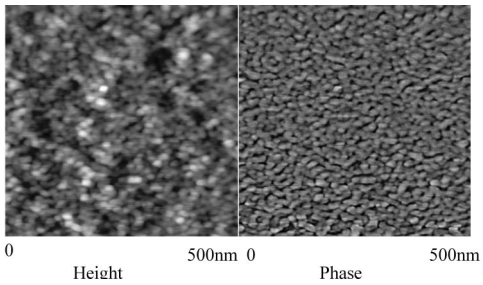

Fig. 1 AFM height (left) and phase (right) data for oriented PET film surface. The *z*-scales are 0–10 nm and 0–20 degrees, respectively, and the scan boxes are 500×500 nm. White is high in topography and also corresponds to high stiffness regions in the phase data. The film machine direction is horizontal

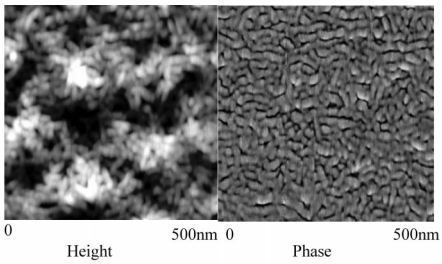

Fig. 2 AFM height (left) and phase (right) data for oriented PEN film surface. The *z*-scales are 0–10 nm and 0–20 degrees, respectively, and the scan boxes are 500×500 nm. White is high in topography and also corresponds to high stiffness regions in the phase data. The film machine direction is horizontal

formation to the phase data except the contrast is slightly worse in the plots, but there is extra information on micro-crystalline aggregates in the height data which can be seen in Fig. 2 as clusters of about 10–20 lamellae. The domains are seen to be smaller in oriented PET in Fig. 1 compared to oriented PEN in Fig. 2, and details of sizes and area fractions of crystal domains will be discussed below. From the line scan analysis, the average height of the crystals from dark to light is 0.6±0.2 and 1.0±0.3 nm, and in phase 7±1 degrees and 8±1 degrees for PET and PEN, respectively.

Total crystallinity, extent of crystal reorganization, and many other properties can be extracted from thermal analysis of oriented and non-oriented systems [4, 6, 11–13]. Here DSC and TMDSC are combined with an independent rapid heating rate technique to characterize properties of these materials. The temperature at which the sample first completely flows when heated at ultra-fast heating rates to prevent reorganization, is a measure of a melting point equivalent to the end of melting of crystals originally present in the sample ($T_{m, rapid}$). For amorphous PET and PEN the respective polymers flow just above T_g because there are no crystals (Figs 3a and 4a for the respective glass transitions). For oriented PET and PEN in Figs 3b and 4b, respectively, $T_{m, rapid}$ is surprisingly low (indicated by arrow in plots), dramatically illustrating the effect of recrystallization during the thermal scan on inducing artificially high DSC final melting endotherms. Note that $T_{m, rapid}$ is equal to 244±2°C for oriented PET while the final DSC melting point from the endotherm in Fig. 3b is 258°C, and for oriented PEN, $T_{m, rapid}$=255±2°C while the DSC value is 268°C (Fig. 4b). Looking at the total DSC curves in Figs 3b and 4b there is little indication of the massive recrystallization that causes the high DSC melting points, but the NR-TMDSC curves show quite dramatically the exothermic recrystallization events in the vicinity of the final melting endotherm, and this is evidence of the large extent of recrystallization. The same trend was found in the previous TMDSC study [15], and earlier by quenching experiments [7]. The endothermic 'pre-melting' partially compensates the exotherm giving the observed total DSC curve where no exotherm is detected (Figs 3b and 4b). The integrated quantities including heats of fusion are given in Table 1.

The data for oriented PET (Fig. 3b) can be contrasted with those for an isothermally (195°C,1 h) melt crystallized PET sample (Fig. 5a). Again, the NR-exothermic recrystallization peak occurs in the vicinity of the rapid heating rate value of the end of melting of originally present crystals ($T_{m, rapid}$), and the recrystallization occurs mainly after the annealing temperature of 195°C as expected since below this temperature the crystals are relatively stable. What is somewhat unexpected is the large level of melting and recrystallization occurring continuously from 200°C to the end of the final melting region in Fig. 5a [15], none of which is evident from the total DSC signal because of offsetting exothermic and endothermic activity. The process of melting has been discussed in a related TMDSC study [15] of PEN and PEEK. Just above the annealing temperature of 195°C in Fig. 5a, melting of secondary crystals begins. Melting of the broad primary crystals continues up to about 240°C, which is about the mean melting point of the primary crystals, and these primary crystals also completely melt and recrystallize especially at temperatures around the large NR exothermic transition between 230°C and 250°C . Both the secondary and primary crystals were mostly formed during the 195°C isothermal anneal [14]. The massive recrystallization of primary crystals is not clear in

standard DSC, but with improved interpretation it is well characterized by the TMDSC 'recrystallization exotherm' at 256°C (Fig. 5a). This recrystallization peak and its importance on the macroscopic properties is verified by the rapid heating rate measurement

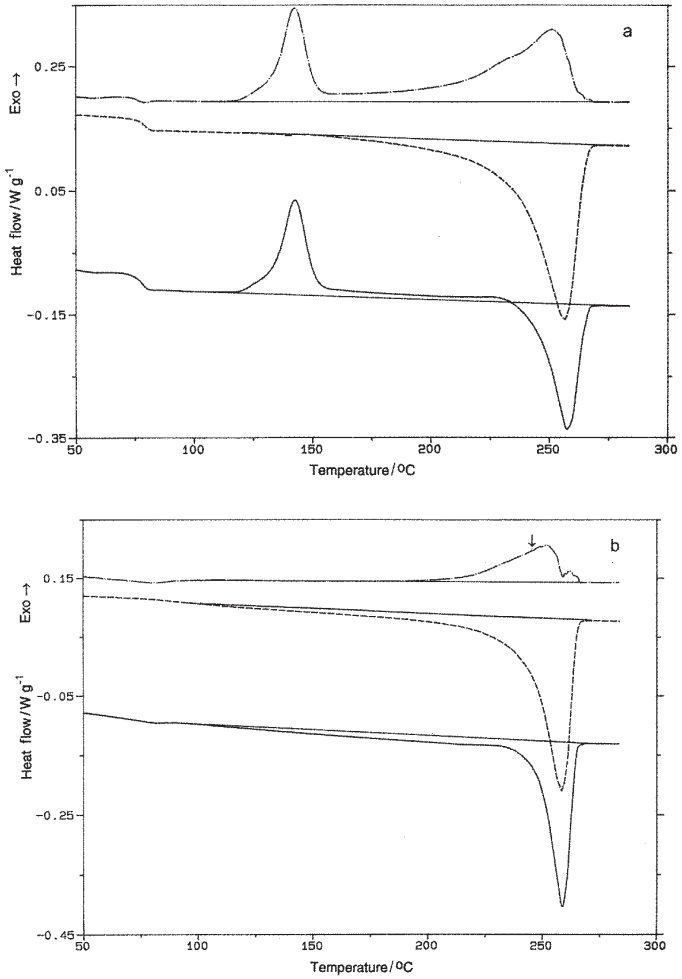

Fig. 3 Total (solid curve), reversing (dashed) and non-reversing (dot-dash) TMDSC data at 3.5°C min^{-1} heating rate for initially amorphous PET. The total signal is the sum of the R and NR signals. The curves have been shifted vertically for clarity. The total signal is equivalent to a standard DSC curve, even though it was obtained in a TMDSC experiment (a). Total (solid curve), reversing (dashed) and non-reversing (dot-dash) TMDSC data for oriented PET at 3.5°C min^{-1} heating rate. The curves have been shifted vertically for clarity. The melting temperature of crystals 'originally' present equals 244°C and was independently measured by the rapid heating rate technique discussed in the Experimental, and this temperature is indicated by the arrow on the plot (b)

which gives a melting point of 242±3°C, which is equivalent to the melting of the originally present primary crystals.

Returning to the data for amorphous systems, the NR-TMDSC (and total DSC) data show the usual cold crystallization exotherm as a sharp event above T_g. Although not clear in the total curve, the NR data show a finite level of exothermic activity con-

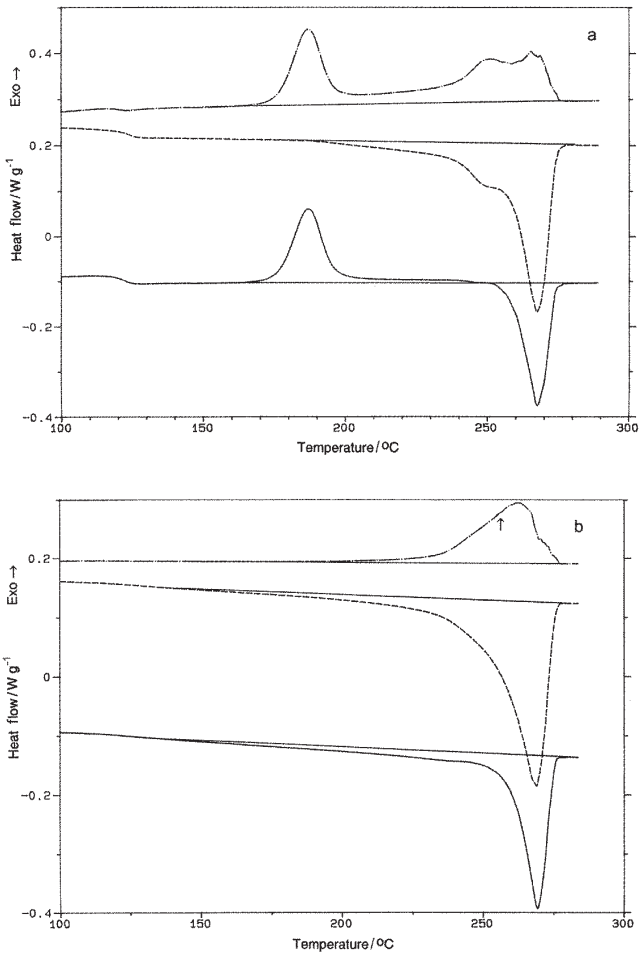

Fig. 4 Total (solid curve), reversing (dashed) and non-reversing (dot-dash) TMDSC data at 3.5°C min^{-1} heating rate for initially amorphous PEN. The curves have been shifted vertically for clarity. The total signal is the sum of the R and NR signals (a). Total (solid curve), reversing (dashed) and non-reversing (dot-dash) TMDSC data for oriented PEN at 3.5°C min^{-1} heating rate. The curves have been shifted vertically for clarity. The melting temperature of crystals 'originally' present equals 255°C and was independently measured by the rapid heating rate technique discussed in the Experimental, and this temperature is indicated by the arrow on the plot (b)

sisting of further crystallization of amorphous areas, i.e., more cold crystallization which occurs slightly above the sharp exotherm normally considered as the main cold crystallization region. This crystallization is combined with recrystallization above

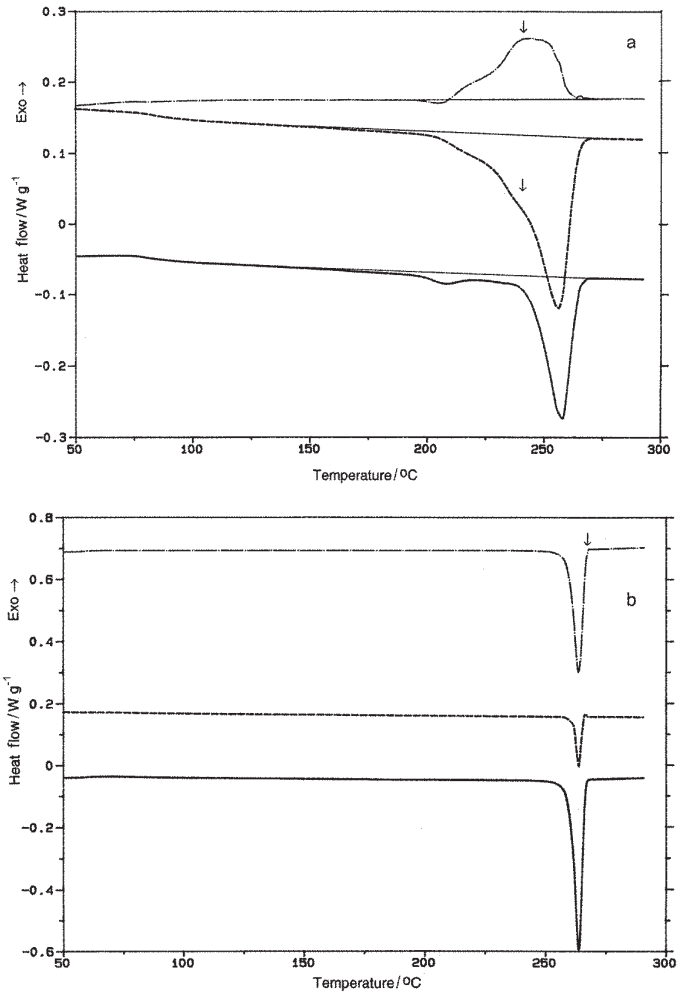

Fig. 5 Total (solid curve), reversing (dashed) and non-reversing (dot-dash) TMDSC data at 3.5°C min^{-1} heating rate for PET annealed at 195°C for 1 h. The curves have been shifted vertically for clarity. The melting temperature of crystals 'originally' present equals 242°C and was independently measured by the rapid heating rate technique, and this temperature is indicated by the arrows (a). Total (solid curve), reversing (dashed) and non-reversing (dot-dash) TMDSC data at 2°C min^{-1} heating rate for PET annealed at 231°C for 24 h. The curves have been shifted vertically for clarity. The melting temperature of crystals 'originally' present equals 269°C and was independently measured by the rapid heating rate technique, and this temperature is indicated by the arrow (b)

the sharp exotherms at 142°C and 186°C for PET and PEN in Figs 3a and 4a, respectively. Recrystallization of these low melting defective crystals dominates about 40°C above these sharp peaks. The early melting detected in the reversible signal starts at about 150°C for PET and 180°C for PEN and occurs at a low enough degree of undercooling that those species which melted just above 150°C and 180°C, can readily recrystallize and contribute to the broad NR-exotherm above these respective temperatures. Especially near the second exothermic peaks in Figs 3a and 4a, the massive recrystallization of the crystals originally formed in the sharp lower temperature exotherm is detected. Again, recrystallization causes a relatively high final melting endotherm, not too far from the final endotherm for many of the other isothermally crystallized or stress crystallized systems studied here (Figs 3b, 4b, 5a).

The higher recrystallization exotherms for the oriented systems in Figs 3b and 4b are smaller than those obtained for the respective amorphous samples in Figs 3a and 4a, respectively, and the cold crystallization exotherms about 50°C above T_g are completely absent in the oriented films as expected since they are already crystallized. Most importantly, the level of rearrangement with increasing temperature is characterized in detail by the novel TMDSC data combined with the rapid heating rate technique.

One can obtain insight into the relationship of TMDSC characterization and crystal stability by examination of long-time, high temperature crystallized PET or related polyesters. Consider a morphology which is stable to recrystallization during the DSC measurement, i.e., a close to a zero entropy production melting process [2]. This topic has been reviewed in detail [2]. One example is given in Fig. 5b for PET annealed at 231°C for 24 h. The standard (total) signal shows a sharp endotherm with a melting point of 263°C, and the non-reversing data show no hint of a recrystallization exotherm before the final melting region. Most of the endotherm is NR because of contributions of the slow melting kinetics to the modulated heat flow profile at the zero heating rate part of the cycle [29]. Because of the large NR endotherm, there is only a small contribution to the reversing endotherm. The melting point of crystals originally present determined by the rapid heating rate technique is 268±3°C, which agrees well with the end of melting determined by DSC in Fig. 5b. This proves that this is one thermal history which results in melting of species present in the original sample which are not affected significantly by the heating scan.

Discussion

On average the hard domains in oriented PET (Fig. 1) characterized by AFM are 11×30 nm while in oriented PEN (Fig. 2) the domains are 21×45 nm. AFM contrast is from modulus differences and it is likely that hard domains consist of both crystal and rigid interphase species since there is no way to distinguish between the two. The orientation of the three dimensional domains below the surface relative to the plane of the surface will also tend to make the surface area fraction higher than it actually is in the bulk, but we will ignore this to a first approximation. The differences in domain size are consistent with the larger long period (L) determined by small angle X-ray as

the average spacing between lamellae in isotropic crystallized polymers. For example, L =11.5 nm and L=13.3 nm for PET and PEN, respectively, for relatively low temperature crystallized non-oriented systems [13].

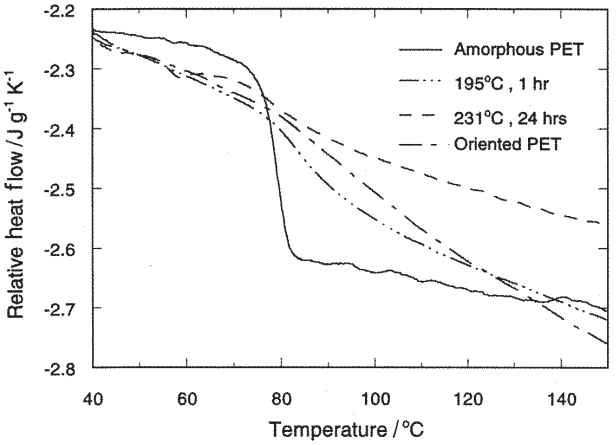

Fig. 6 Reversing TMDSC data showing glass transitions for PET samples

The strength of the glass transition is measured in terms of the step in heat capacity (ΔC_p) obtained from the reversing-TMDSC signal. Figure 6 gives data for the PET samples studied here. The step-size was calculated as described earlier [4, 34] and is a measure of the total rigid fraction (F_{rigid}).

$$F_{rigid} = 1 - \Delta C_p / \Delta C_{p,\,amorphous} \quad (1)$$

where ΔC_p is the measured quantity for the semi-crystalline sample, and F_{rigid} is equivalent to the fraction which cannot contribute to the glass transition, and consists of both crystal fraction (Wc) and 'rigid amorphous' fraction (F_{RAF}). Thus,

$$F_{rigid} = Wc + F_{RAF} \quad (2)$$

Measuring Wc from DSC total ΔH_f using Wc=$\Delta H_f/\Delta H_{f,o}$ and F_{rigid} from ΔC_p, allows one to determine F_{RAF} [4, 18]. Accurate values of Wc are needed, and because of the difficulties in obtaining accurate values of $\Delta H_{f,o}$ *discussed earlier, the lack of accuracy of* $\Delta H_{f,o}$ probably contributes to most of the error. It is known that ΔC_p can be obtained with better accuracy by the TMDSC reversing signal than with standard DSC [4], which improves this part of the analysis for broad and weak glass transitions.

Returning to F_{rigid}, the DSC values for oriented PET and PEN (Table 1) are 0.73±0.05 and 0.85±0.05, while computer processing of the area fraction of hard domains from the AFM phase data gives 0.64±0.07 and 0.79±0.07 for PET and PEN, respectively. The error for the AFM calculations is estimated based on the differences observed depending on the methods chosen to contrast the different hard and soft regions. The differences between PET and PEN are mostly due to the larger size of hard

domains in PEN, with relatively constant soft boundary dimensions. These amorphous domains or boundaries (dark regions) are about 4 nm wide for both systems in Figs 1 and 2. Comparing with the DSC rigid fractions, the trend is correct, although the AFM values are a few percent lower. As discussed earlier, F_{rigid} from DSC accounts for both rigid interphase and crystal volume fraction, and the fact that the AFM hard area fractions are much higher than *Wc*, indicates that the interphase fraction also contributes to the hard phase in the AFM data apparently because the interphase is stiff enough to cause its contrast to be similar to that of crystal.

We now turn to the final topic related to morphology and interphase properties of semi-crystalline systems with and without orientation. According to Eq. 2, one can calculate F_{RAF} using reliable values of F_{rigid} and *Wc* determined by TMDSC. Values of F_{RAF} are 0.28 and 0.50 for oriented PET and PEN respectively, while they are 0.33 and 0.39 for isothermally crystallized PET (195°C) and PEN (190°C), respectively (Table 1). These values are higher than those presented for PEN earlier [12, 18] for reasons discussed below, but the values for PET are quite consistent with those calculated using similar TMDSC data and the same value of $\Delta H_{f,o}$ [4]. The data suggest that the interphase fraction is similar for oriented and isotropic PET samples chosen here, but that the lamellae or lamellar stacks in oriented PEN have a broader interphase region compared to those in isotropic PEN. A higher surface area of crystallites in oriented PEN would also explain some of the differences.

PEN has higher values of F_{RAF} than PET for both isotropic and oriented, maybe because its stiffer chain nature causes more difficulty in forming smooth crystal surfaces, or the stiff chains exiting the crystals in PEN are more restricted. We used the same method of calculating F_{RAF} as presented earlier [18], but on different systems and using some different parameters. Earlier studies [18] considered a series of oriented PEN samples at different extension ratios. In general, the crystallinity is much higher for our oriented PEN due to higher stress crystallization temperatures for our sample (~200°C *vs.* 145°C [18]). The ΔC_p for our sample was also much smaller indicating a much larger F_{rigid}. Most importantly, for the calculations we used $\Delta H_{f,o}$= 170 J g^{-1} for PEN, while $\Delta H_{f,o}$=102.5 J g^{-1} was used previously [18], which results in much higher total crystallinities (*Wc*), and substantially reduces the calculated F_{RAF} relative to ours in Table 1. These issues are not completely resolved, and characterization of a variety of systems with different thermal histories using several methods will improve our understanding in the future.

We can also relate F_{RAF} and F_{rigid} to various morphological models [35, 36]. The very high F_{rigid}=0.9 for the long-time crystallized (24 h, 231°C) PET sample in Table 1, can be compared with the volume fraction of lamellar stacks calculated for a similar isotropic sample [14] using

$$F_{stacks} = Wc\ (lc + la) / lc = 0.52\ (6.6 + 4.3) / 6.6 = 0.85 \quad (3)$$

where *lc* and *la* are the crystal and amorphous layer thicknesses obtained from the correlation function analysis of small angle X-ray scattering data [14]. This suggests that all species within *la* and *lc* do not contribute to the glass transition [35, 36], thus

the species which do contribute are those outside the lamellar stacks in 'gaps' between stacks. Thus, all species within the stacks (i.e., within *la*) are rigid interphase or crystal species. Other evidence supports the presence of such amorphous gaps between stacks, and such gaps would form naturally due to the high degree of topological and conformational constraints encountered during crystallization. We feel this is a reasonable picture due to the very small value of *la* [14, 35, 36] on the order of 3–4 nm, the high level of constraints on interphase species within *la*, given the large length-scale of cooperative glass transition-like motions [37].

Stress-crystallization may lead to better space-filling of crystallites, thus the morphology derived from AFM (Figs 1 and 2) for oriented films paints a different picture. It suggests that the glass transition does arise from amorphous species between crystallites, (Dark regions in figures) because the stress crystallization conditions apparently lead to higher nucleation and to an absence of larger gaps between stacks or aggregates of crystallites. This assumes that the surface morphology from AFM is representative of the bulk morphology. Such a model is consistent with the larger level of constraints causing an elevated T_g in oriented PET (94°C) compared to 77°C for amorphous PET (Table 1), and even 78°C for the highest crystallinity PET sample with the weakest glass transition which is not changed significantly in temperature apparently because the 'gaps' [35, 36, 38] are large enough that the cooperative motions are not significantly affected. The trend is not obvious with PEN although oriented PEN does have a 6°C higher T_g than amorphous.

Conclusions

In TMDSC data for isothermally crystallized isotropic samples the melting of secondary crystals in the low endotherm region is followed by recrystallization which broadly overlaps with melting of primary crystals, with a final endotherm due to melting of the recrystallized species. In oriented films, a similar sequence of events is measured in TMDSC, except because of the non-isothermal stress crystallization conditions there is no low endotherm, but simply a gradually increasing low temperature melting and recrystallization. TMDSC and independently measured melting points of the temperature of complete melting of the original crystals, determined by the rapid heating rate technique discussed in the Experimental, verify the interpretation of TMDSC.

AFM images of crystal morphology on oriented PET and PEN films with nanometer lateral resolution showed details of crystal size and orientation with much smaller crystals detected in PET. The area fractions of rigid species (crystal plus rigid interphase) determined by AFM were consistent with those total rigid fractions (F_{rigid}) determined by DSC. Rigid amorphous fractions (F_{RAF}) were calculated using TMDSC data and a new determination of $\Delta H_{f,o}$ for PEN. Generally F_{RAF} was larger for PEN than PET possibly due to differences in morphology and chain stiffness. The rigid fractions for high crystallinity PET are consistent with previous results [4].

* * *

We thank Dr. J. Siddiqui of DuPont for his important contributions.

References

1 J. M. Schultz and S. Fakirov, 'Solid State Behavior of Linear Polyesters and Polyamides', Prentice Hall, Inc. Englewood Cliffs, New York 1990.
2 B. Wunderlich, Macromolecular Physics, Volume 3, Academic Press, New York 1980.
3 M. Reading, Trends Polym. Sci., 8 (1993) 248. M. Reading, D. Elliot and V. L. Hill, J. Thermal Anal., 40 (1993) 949.
4 I. Okazaki and B. Wunderlich, J. Polym. Sci., Polym. Phys., 34 (1996) 2941.
5 I. Okazaki and B. Wunderlich, Macromol. Rapid Commun., 18 (1997) 313.
6 I. Okazaki and B. Wunderlich, Macromolecules, 30 (1997) 1758.
7 H. G. Zachmann and H. A. Stuart, Makromol. Chem., 8 (1960) 131.
8 P. J. Holdsworth and A. Turner-Jones, Polymer, 12 (1971) 195.
9 G. Groeninckx, H. Reynaers, H. Berghmans and G. Smets, J. Polym. Sci., Polym. Phys., 18 (1980) 1311.
10 C. Zhou and S. B. Clough, Polym. Eng. Sci., 28 (1988) 65.
11 S. Buchner, D. Wiswe and H. G. Zachmann, Polymer, 30 (1989) 480.
12 S. Z. D. Cheng, M.-Y. Cao and B. Wunderlich, Macromolecules, 21 (1988) 789.
13 F. J. Medellin-Rodriguez, P. J. Phillips and J. S. Lin, Macromolecules, 29 (1996) 7491.
14 Z. G. Wang, B. S. Hsiao, B. B. Sauer and W. G. Kampert, Polymer, 40 (1999) 4615.
15 B. B. Sauer, W. G. Kampert, E. N. Blanchard, S. A. Threefoot and B. S. Hsiao, Polymer, 41 (2000) 1099.
16 C. Fougnies, P. Damman, M. Dosiere and M. H. Koch, J. Macromolecules, 30 (1997) 1392.
17 G. Qiu, Z.-L. Tang, N.-X. Huang and L. Gerking, J. Appl. Polym. Sci., 69 (1998) 729.
18 S. Z. D. Cheng, J. J. Janimak, A. Zhang, J. Guan and A.-L. Chu, Polymer Bulletin, 20 (1988) 449.
19 S. N. Maganov and M.-H. Whangbo, 'Surface Analysis with STM and AFM VCH', VCH Publishers, Weinheim 1996.
20 R. S. McLean and B. B. Sauer, Macromolecules, 30 (1997) 8314.
21 S. Magonov and Y. Godovsky, Amer. Lab., 31 (1999) 52.
22 S. A. C. Gould, D. A. Schiraldi and M. L. Occelli, J. Appl. Polym. Sci., 65 (1997) 1237.
23 J. S. G. Ling and G. Leggett, J. Amer. Chem. Soc. Polym. Preprints, 38(1) (1997) 1061.
24 D. J. Blundell and B. N. Osborn, Polymer, 24 (1983) 953.
25 P. Zoller, T. A. Kehl, H. W. Starkweather and G. A. Jones, J. Polym. Sci., Polym. Phys., 27 (1989) 993.
26 J. N. Hay, J. I. Langford and J. R. Lloyd, Polymer, 30 (1989) 489.
27 H. W. Starkweather, P. Zoller and G. A. Jones, J. Polym. Sci., Polym. Phys., 21 (1983) 295.
28 B. Wunderlich, in 'Thermal Analysis', Academic Press, New York 1990.
29 L. C. Thomas and S. R. Aubuchon, to be published, 1999. Software provided by T.A. Instruments, Inc. 109 Lukens Drive, New Castle, DE 19720.
30 K. Ishikiriyama and B. Wunderlich, Macromolecules, 30 (1997) 4126.
31 Q. Zhong, D. Inniss, K. Kjoller and V. B. Elings, Surface Sci. Lett., 290 (1993) L688.
32 G. Bar, Y. Thomann and M.-H. Whangbo, Langmuir, 14 (1998) 1219.
33 R. S. McLean and B. B. Sauer, J. Polym. Sci., Polym. Phys., 37 (1999) 859.
34 S. Z. D. Cheng, M.-Y. Cao and B. Wunderlich, Macromolecules, 19 (1986) 1868.
35 B. B. Sauer and B. S. Hsiao, Proceedings of the Amer. Chem. Society, Division of P.M.S.E., 69 (1993) 35.
36 B. B. Sauer and B. S. Hsiao, Polymer, 35 (1995) 2553.
37 E. J. Donth, Non-Cryst. Solids, 53 (1982) 325.
38 C. Santa Cruz, N. Stribeck, H. G. Zachmann and F. J. Balta Calleja, Macromolecules, 24 (1991) 5980.